applied optics

Pitfalls in the spectral measurements of polarization-altering metasurfaces

Hsiang-Chu Wang and Olivier J. F. Martin*

Nanophotonics and Metrology Laboratory, Swiss Federal Institute of Technology Lausanne (EPFL), 1015 Lausanne, Switzerland
**Corresponding author: olivier.martin@epfl.ch*

Received 4 July 2022; revised 31 August 2022; accepted 2 September 2022; posted 2 September 2022; published 19 September 2022

The optical characterization of metasurfaces and nanostructures that alter the polarization of light is tricky and can lead to unphysical results, such as reflectance beyond unity. We track the origin of such pitfalls to the response of some typical optical components used in a commercial microscope or a custom-made setup. In particular, the beam splitter and some mirrors have different responses for both polarizations and can produce wrong results. A simple procedure is described to correct these erroneous results, based on the optical characterization of the different components in the optical setup. With this procedure, the experimental results match the numerical simulations perfectly. The methodology described here is simple and will enable the accurate spectral measurements of nanostructures and metasurfaces that alter the polarization of the incoming light.

https://doi.org/10.1364/AO.469399

1. INTRODUCTION

Since its inception in the 17th century, the optical microscope has become the key instrument to investigate light–matter interactions [1]. Over the last decade, the optical microscope has enabled the development of metasurfaces: artificial optical components built from sub-wavelength nanostructures, the so-called meta-atoms [2–6]. Here, by optical microscope, we refer to any type of platform, from the most sophisticated commercial device to its simplest counterpart built from an illumination path, a sample holder, an objective, and a tube lens.

Among the methods demonstrated, the meta-atom geometries and materials play a key role in determining the metasurface function. The geometries come in a variety of shapes. For the materials, plasmonic metals [7–9], or high permittivity dielectrics [10–19] are utilized, with some emerging alternative routes, such as hybrid meta-atoms that combine metal and dielectrics [20–22], or alloyed nanostructures [23].

To mimic classical optical elements, metasurfaces usually manipulate the phase of light which, in turn, requires manipulating its polarization [24]. Hence, most metasurfaces produce reflected or transmitted light with a polarization that is different from that of the incoming light. This polarization altering can cause some difficulties when measuring metasurfaces in an optical microscope, and the objective of this paper is to document those difficulties and describe workarounds. Figure 1 shows some popular metasurfaces that are sensitive to polarization: (a) beam-steering devices utilizing phase gradients that operate only for a specific polarization direction [25–27]; (b) a metalens that uses the Pancharatnam–Berry (PB) phase and is excited with a given circular polarization, while the resulting light phase has the opposite handedness [28–31]; (c) and even structures that alter the incident polarized light into another polarization [32–36]. From these examples, we observe that the corresponding meta-atoms have a low symmetry, such as a rectangular shape that responds differently to incident orthogonal polarizations [37] and causes complications in their optical characterization. For completeness, we must also mention another class of metasurfaces that are built from high symmetry meta-atoms, for example, disks, and are polarization insensitive [23,38–40]. We are not concerned with such metasurfaces in this work.

The paper is organized as follows: in Section 2, we describe a typical microscope setup for the spectral measurement of metasurfaces; in Section 3, we compare numerical simulations with measurements on effectively fabricated metasurfaces and explain the origin of the discrepancies between the two. Next, a simple procedure is described to correct such discrepancies and we conclude in the final section.

2. OPTICAL MICROSCOPE SYSTEM

The custom-built microscope system used in this work is shown in Fig. 2; it is constructed around a commercial inverted optical microscope and includes a spectrometer and a camera. Our aim is to measure the metasurface spectral response over the entire visible range and compare it with numerical simulations. Indeed, during the design of a metasurface, full-wave simulations are used to compute the amplitude and phase produced by a meta-atom. Here we resort to Comsol Multiphysics Version 5.6 for this task. For numerical simulations, it is straightforward to select one specific illumination polarization and then analyze the polarization of the scattered light: this process is entirely

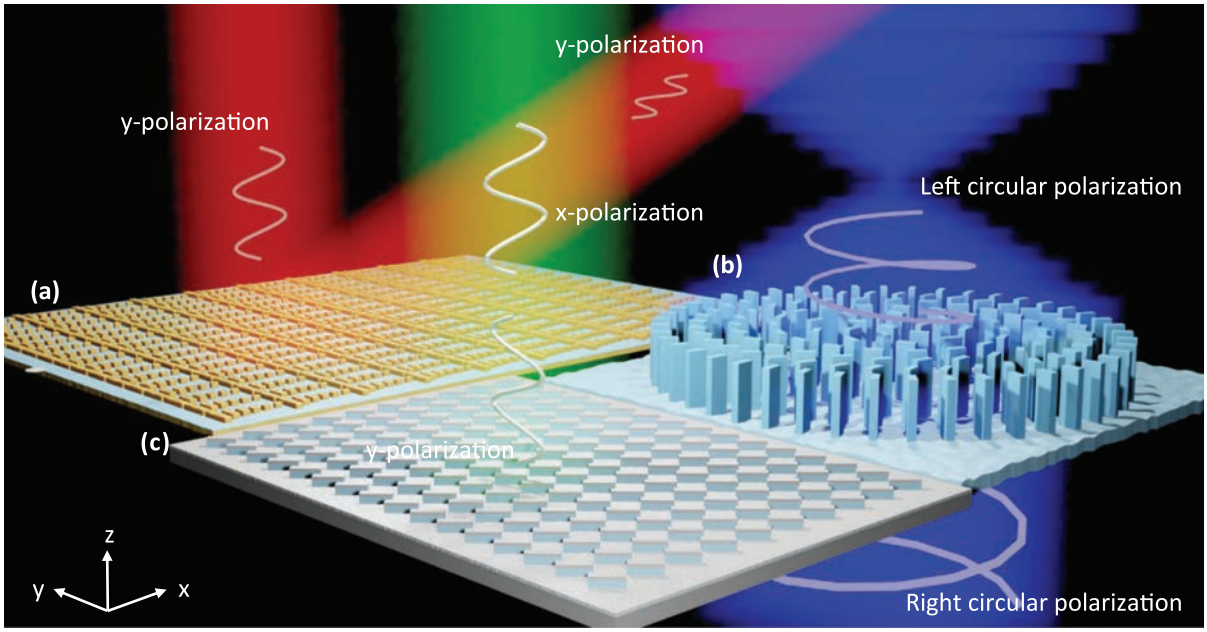

Fig. 1. Examples of metasurfaces and the way they modify the polarization of light. (a) Polarization-sensitive meta-atoms for wavefront manipulation, requiring specific polarized light for excitation and detection. (b) Metalens based on the PB phase that transforms right circular polarization into left circular polarization, and vice versa. (c) Structural metasurface built from protruding nanorods rotated by 45° that convert white light into a specific color upon reflection.

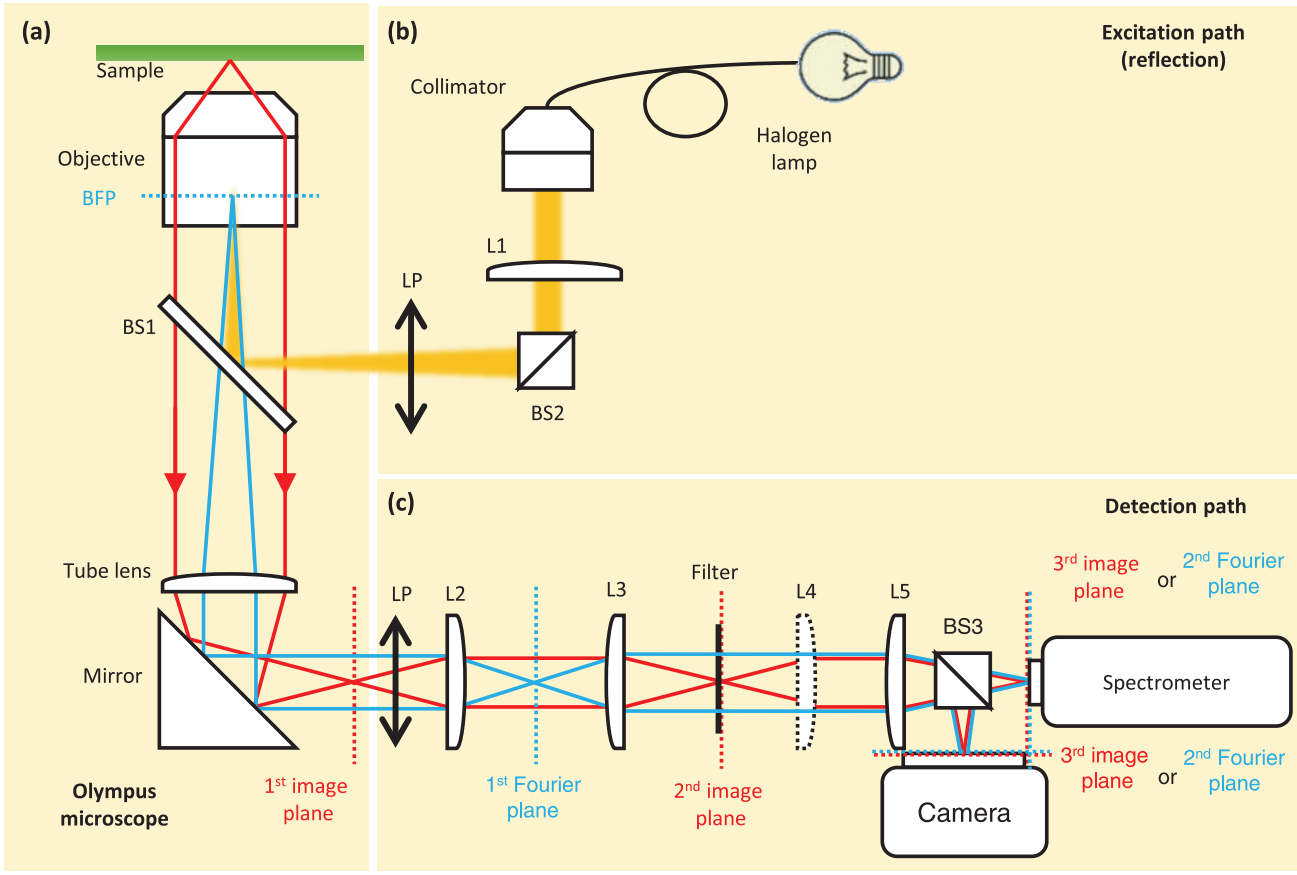

Fig. 2. Schematic of the optical system for measuring the spectrum of metasurfaces under polarized illumination. (a) Schematic of an inverted microscope (Olympus IX73). (b) Excitation path by a halogen lamp in reflection type. (c) Detection path composed of a 4f system and a spectrometer with a CCD camera.

numerical and requires only projecting the electromagnetic field on a basis, such as the Jones vectors to obtain the amplitude, phase, and polarization of the scattered light [41]. The procedure is more complicated in an experiment since physical components such as polarizers, analyzers, beam splitters, mirrors, and wave plates must be used, and these components have a response that changes over the spectral range of interest [24].

The measurement setup shown in Fig. 2 is operated in the reflection mode, with two additional key components: a linear polarizer (LP) in the excitation path and an analyzer (LP) in the detection path. By adding these two LPs, we intend to illuminate the metasurfaces with linearly polarized light and analyze the polarization states of reflected light. This system can be separated into three parts: the optical microscope in Fig. 2(a), the illumination in Fig. 2(b), and the detection in Fig. 2(c). The microscope is an inverted microscope (Olympus, IX73) composed of four components: a 50/50 plate beam splitter (Chroma, AHF F21-020), an objective (LUCPLFLN 60×, NA = 0.7), a tube lens, and a dielectric mirror. When the halogen lamp is on, light first couples into the fiber and becomes collimated by the collimator (Objective 10× air). Afterwards, the lens L1 (Thorlabs, LA1172-A) and LP (Thorlabs, WP25M-UB) are used to focus the beam at the back focal plane of the objective, producing a plane wave excitation on the sample metasurface. To ensure normal incidence, in the Fourier plane on the camera (Flir, CM3-U3-50S5C-CS), we ensure that the beam is at the center of the objective. Light reflected by the sample is collected by the same objective with NA = 0.7. The NA indicates the angle θ up to which the scattered light can be coupled into the objective: $\mathrm{NA} = n\sin(\theta)$, where n is the refractive index of the environment (air in this case, $n = 1$). Hence, the scattered light between $\pm 44.4^{\circ}$ can be collected by the objective. After passing the 50/50 plate beam splitter, the sample image is projected on the first image plane with the assistance of the tube lens, and the dielectric mirror belonged to the microscope. Generally, a camera is placed at the exit of the microscope for imaging. In contrast, here we put the LP (Thorlabs, WP25M-UB) instead to analyze the polarization state of the reflected light. Besides, we implement a 4f system for post-processing the image in the first image plane. When the lens L4 in Fig. 2(c) is removed, images on the Fourier planes, such as the BPF of the objective and the first Fourier plane will be projected onto the second Fourier plane. On the other hand, the first and second image planes will be projected onto the third image plane when all the lenses are in place. This 4f imaging system is optimized with four lenses L2–L5 (Thorlabs, LA1979-A, LA1979-A, LA1131-A, LA1608-A) for special-selective spectral measurements, high-pass or low-pass imaging, and Fourier plane imaging. Here we only need to analyze the spectrum of the sample under polarized illumination, so we use this 4f system only to extend the image onto the spectrometer with the LP on the first image plane to analyze the polarization.

Building the measurement setup from a commercial microscope provides stability, robustness, and positioning accuracy, which is important for small samples, such as metasurfaces; on the other hand, there might be some "hidden" optical components within the microscope body that require detailed characterization to fully understand the optical path within the microscope.

3. METASURFACE MEASUREMENTS

We consider a metasurface built from a silver nanorod, which has been used by several authors [42–49]. This simple geometry exhibits a chirality that arises from the polarization of the incident light, as soon as it is not parallel to one of the structure's symmetry axes [50]. When this is the case, part of the incident polarization is converted into the orthogonal polarization, producing a dichroic response. We will show that special care must be taken when measuring such a metasurface and unexpected, polarization-related, effects might occur in the experiment, which are not present in the full-wave simulation since, for the latter, there are no additional polarization-sensitive optical components, such as mirrors or beam splitters to retrieve the optical signal.

The schematics of the meta-atom are described in the inset of Fig. 3(a): it is a rectangular silver rod ($W = 40$ nm, $L = 110$ nm) inside a square lattice with period $P = 300$ nm in both directions. A 150 nm thick negative photoresist HSQ (DuPont, hydrogen silsesquioxane) written with electron beam lithography defines the nanostructure on a Si substrate. 40 nm thick silver is evaporated (Leybold Optics, LAB 600H) on the entire structure, producing an Ag nanorod that protrudes from an Ag background with complementary geometry. This simple fabrication approach has been used to build a variety of plasmonic nanostructures and metasurfaces [51–60]. This meta-atom is illuminated with polarized (x or y polarizations) light propagating in the z direction, while the reflected light is collected with an analyzer (x or y polarizations). This leads to four combinations of reflectance spectra obtained from the combinations of incident and reflected lights: R_{xx}, R_{xy}, R_{yy}, and R_{yx}. The first indices indicate the incident polarizations, while the second indices indicate the analyzer directions. Figure 3(a) shows the simulated spectra when the rod is aligned with the x direction; R_{xx} and R_{yy} are present, while R_{xy} and R_{yx} vanish. The corresponding measurements, shown in Fig. 3(b), together with the scanning electron microscope (SEM) image of the sample, agree well with the calculations. To distinguish between calculated reflectance and measured reflectance, we describe the latter with subscripts that correspond to the polarization used in the experiment: R_{ss} (corresponding to R_{xx}), R_{sp} (R_{xy}), R_{pp} (R_{yy}), and R_{ps} (R_{yx}).

When the rod is rotated by 45°, the cross-polarization term R_{xy} appears in the calculations; see Fig. 3(c). This cross-polarization term indicates that the metasurface exhibits chirality when the incident polarization is not parallel to the meta-atom axes [50]. Besides, the R_{xx} [blue line in Fig. 3(c)] exhibits now a deep trough and behaves in a complimentary way to R_{xy}. Due to the structural symmetry, the spectra R_{xx} and R_{yy} overlap, and so do the spectra of R_{xy} and R_{yx}. This spectral change due to the rotation of the same structure caught our attention, and we measured the original sample rotated by 45°, as indicated in the inset of Fig. 3(d). Surprisingly, unphysical reflectance data are obtained in this case, with a reflectance larger than unity; see Fig. 3(d). This disagreement between simulations and measurement prompted us to investigate the optical responses of the components used in the setup.

It turns out that the optical responses of plate beam splitters are polarization-sensitive, i.e., their transmittance is different

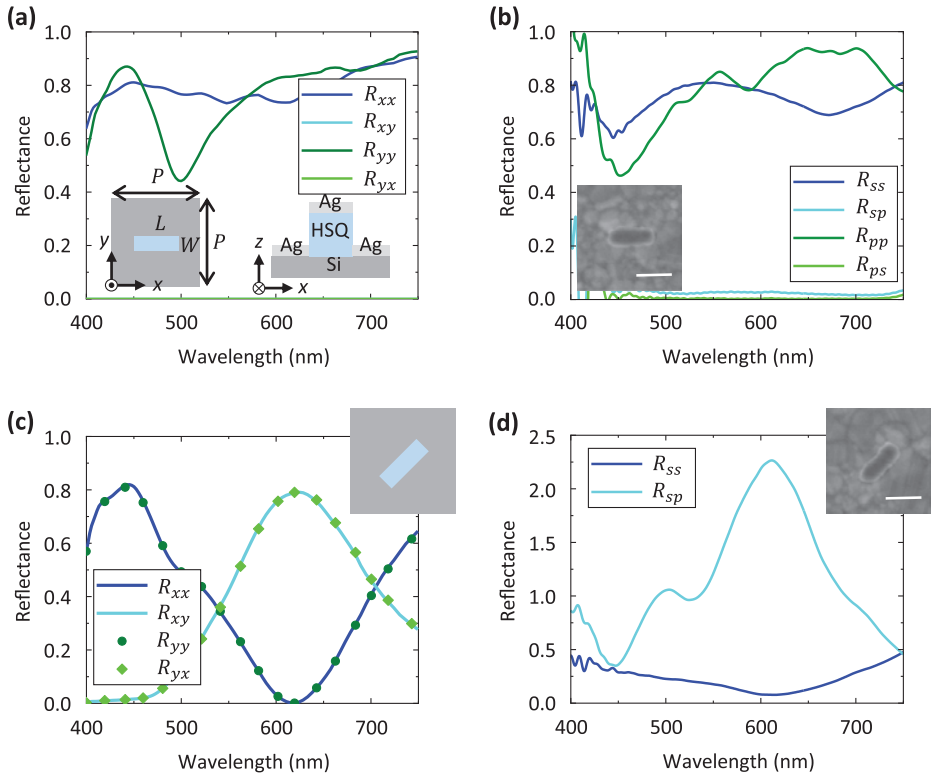

Fig. 3. Simulated and measured spectra for the metasurface built from an array of Ag meta-atom rods. (a) Simulated and (b) measured reflectance spectra when the rods are aligned along the x direction. The insets in panel (a) sketch the meta-atom, while the inset in panel (b) shows the SEM image of the fabricated structure. (c) Simulated and (d) measured reflectance spectra when the sample has been rotated by 45°. (Scale bars: 100 nm).

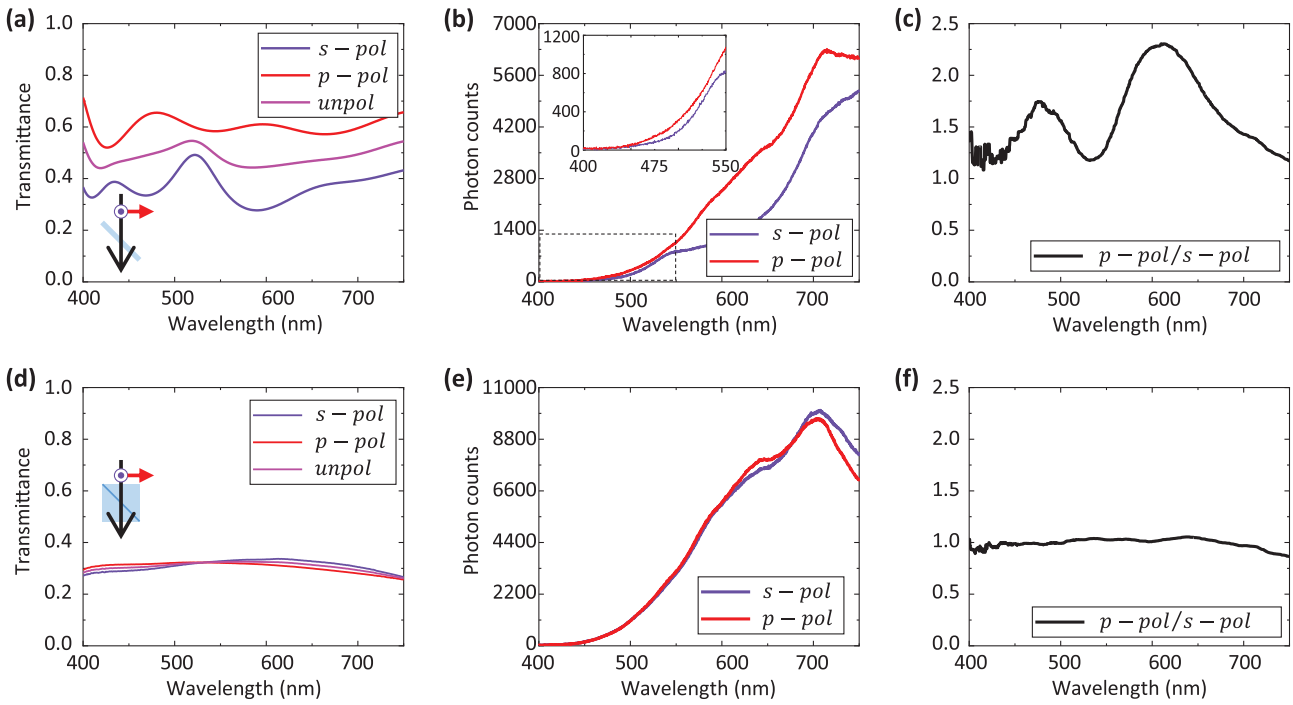

Fig. 4. Comparison between the optical responses in terms of polarizations for a plate beam splitter and a cube beam splitter. (a) Transmittance of the plate beam splitter (Chroma, 50/50 AHF F21-020). (b) Transmittance for polarized light passing this plate beam splitter. (c) Corresponding transmittance ratio. (d) Transmittance of the cube beam splitter (Thorlabs, 70/30 BS022). (e) Transmittance for polarized light passing this cube beam splitter. (f) Corresponding transmittance ratio.

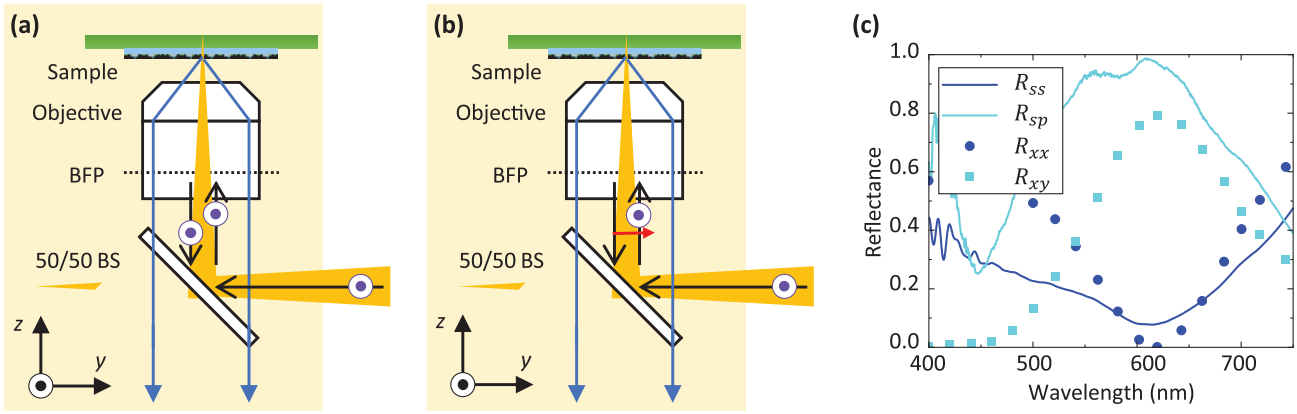

Fig. 5. Schematic of polarized light propagating in a microscope with a polarization-sensitive plate beam splitter. (a) S-polarized light reflected by a sample and the reflected light polarized in the same direction as incident light. (b) S-polarized light reflected by a sample that alters the polarization into p-polarization as reflected. (c) Corrected spectra from measurements compared with the simulated.

for s- and p-polarized light. (S-polarization is defined as the electric field perpendicular to the plane of incidence, while p-polarization has the electric field parallel to the plane of incidence.) The transmittance measured for the plate beam splitter used in our setup (Chroma, 50/50 AHF F21-020) is shown in Fig. 4(a). The transmittance for unpolarized light (magenta line) in Fig. 4(a) is the average of s-polarization (purple line) and p-polarization (red line). This polarization-dependent transmittance gives rise to different intensities depending on the polarization of the light. Even for a halogen lamp with equal intensities in s- and p-polarizations, the measured spectra after the plate beam splitter deviate from each other, as shown in Fig. 4(b): at first sight, the spectra appear are comparable between $\lambda = 400$ and 550 nm, but when magnified they are still different. To quantify this difference, in Fig. 4(c), we plot the intensity ratio for both polarizations. Overall, this ratio is larger than one and exhibits a fluctuation pattern; it indicates that the reflected light for p-polarization can have larger transmittance than for s-polarization. This explains the unphysical data observed in Fig. 3(d): if the incident light is s-polarized and its polarization is converted by the meta-atom, the reflected spectrum will be multiplied by a factor larger than one, producing a response where energy appears to have been generated. We will discuss this in greater detail in the next section. Ideally, the transmittance ratio between both polarizations should be constant to avoid any polarization dependency. It turns out that cube beam splitters do not have such a drawback, as shown in Fig. 4(d), for the element (Thorlabs, 70/30 BS022): the transmittances for each polarization almost overlap. Similar plots to those presented in Figs. 4(b) and 4(c) for the plate beam splitter are shown for the cube beam splitter in Figs. 4(e) and 4(f). In this case, the transmittances for both polarizations are similar, and their ratio is a constant over the visible spectrum. Therefore, a cube beam splitter is a good option for measurements where polarization plays a role. Unfortunately, there are no commercial holders for cube beam splitters to be mounted in commercial microscopes; in our case, we fabricated one using 3D printing. Fortunately, it is still possible to correct the spectrum measured in Fig. 3(d), as will be discussed next.

Let us dwell further into the details of the issues that can arise when measuring with the system shown in Fig. 2, a sample that modifies the incident polarization, e.g., the situation shown in Fig. 3(c) when the sample has been rotated by 45°. Figure 5(a) is the case when the sample reflects light without changing the polarization state. We consider s-polarized incident light with spectrum I_s that is first reflected by the beam splitter, so the spectrum can be expresses as $R_s\ I_s$, where R_s is the reflectance of the beam splitter for s-polarization. We assume that the objective is lossless and polarization-insensitive. This polarized light reached the sample and is reflected without changes of polarization, with R_{ss} being the sample reflectance. Hence, the reflected spectrum becomes $R_{ss}\ R_s\ I_s$ and, after passing through the beam splitter with transmittance T_s for s-polarization, the measured spectrum becomes $M_{ss} = T_s\ R_{ss}\ R_s\ I_s$. The reflectance of a sample is defined as the measured spectrum M_{ss} divided by the incident light. For the inverted microscope, we obtain the incident light by placing a silver mirror with unit reflectance at the location of the sample. Since this silver mirror does not change the polarization of the normal incident light, the reference spectrum measured with the mirror is $M_{ss}^{\mathrm{ref}} = T_s\ R_s\ I_s$ and the sample reflectance R_{ss} is obtained by dividing the spectrum with the sample by that reference spectrum.

On the other hand, considering the case shown in Fig. 5(b) where the sample alters the incident s-polarized light into p-polarization, the measured spectrum becomes $M_{sp} = T_p\ R_{sp}\ R_s\ I_s$, where R_{sp} is the amount of light converted by the sample from s- to p-polarization upon reflection, and T_p is the beam splitter transmittance for p-polarization. If one used the same definition for deriving the sample reflectance R_{sp} and divide the measured spectrum by the reference spectrum, one obtains $R_{sp}\ T_p/T_s$ instead of R_{sp}; the properties of the beam splitter bias the response. However, it is possible to retrieve the correct sample response by dividing the measured spectrum with the ratio T_p/T_s. For example, if one divides the spectrum in Fig. 3(d) with the polarization ratio T_p/T_s shown in Fig. 4(c), one retrieves the correct sample reflectance R_{sp}; see the cyan line in Fig. 5(c). Note that the corrected reflectance R_{sp} shown in Fig. 5(c) recovers around $\lambda = 600$ nm the broad resonance for R_{xy} and the dip for around R_{xx} computed in Fig. 3(c).

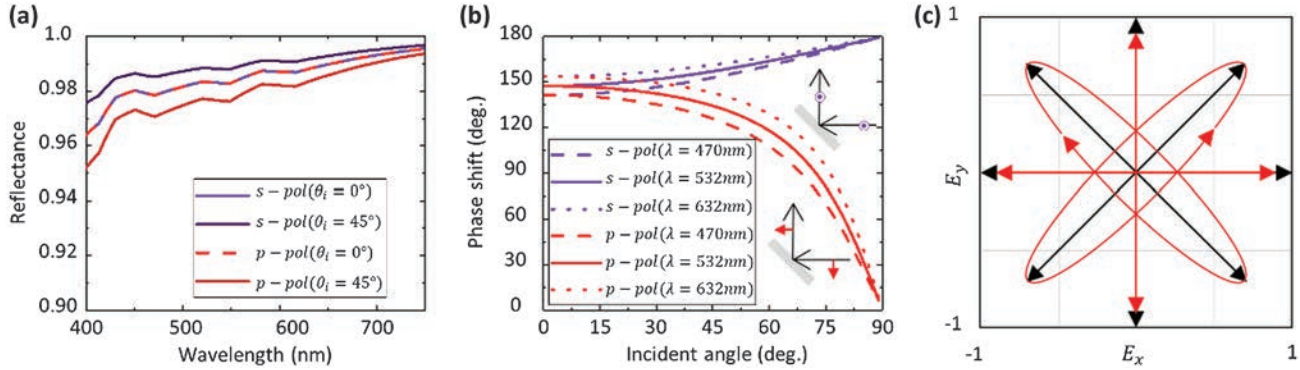

Fig. 6. Reflectance and phase shift for polarized light reflected by a silver mirror derived from Fresnel coefficients. (a) Reflectance spectrum in the visible range for s- and p-polarized light incident at 0° and 45°. (b) Phase shift as a function of the incident angle for s- and p-polarized light at three primary wavelengths. (c) Polarization patterns for the reflected light at $\lambda = 532$ nm for light incident at 45° on a silver mirror for four different incident linear polarizations: s- and p-polarizations are conserved, while diagonal and anti-diagonal incident linear polarizations produce an elliptically polarized plane wave.

In addition to beam splitters, mirrors used in the setup can affect the measurements. For example, silver mirrors serve as perfect reflectors, since they are capable of reflecting the incident light over the entire spectrum, from the visible to the near infrared with little absorption. The reflectance of a silver mirror can be calculated with the Fresnel coefficients [61] using the permittivity from Johnson and Christy [62], as shown in Fig. 6(a) for light incident at 0° or 45°, as is the case of the optical setup used here. At normal incidence 0°, the reflectance overlaps both polarizations. On the other hand, for 45° incidence, the reflectance for s-polarized light increases up to 1% compared to the normal incidence, while it drops up to 1% for p-polarized light. Furthermore, the difference of the phase shift between s- and p-polarized light reflected by the mirror and computed with the Fresnel coefficients increases with the angle of incidence; see Fig. 6(b). As a consequence, when both components are present, the reflected light becomes elliptically polarized. This is illustrated in Fig. 6(c), where we show the polarization ellipse for light reflected from a silver mirror at $\lambda = 532$ nm. The angle of incidence is 45°, and four different polarizations are considered: s- and p-polarizations, which are conserved upon reflection; while diagonal and anti-diagonal polarizations lead to elliptically polarized reflected light. This behavior originates from the complex dielectric function of silver and would not occur with a dielectric mirror. Therefore, when using silver mirrors in a measurement system, polarizations in horizontal and vertical directions can be retained without being modified, while other polarization states need to be handled with care.

4. CONCLUSION

In summary, we have analyzed the fate of polarization as light propagates through a conventional microscope setup used to measure optical nanostructures, metasurfaces, or polarization-altering optical components. When the sample alters the incident polarization, special care must be taken to avoid unphysical effects, such as a reflectance beyond unity or experimental measurements that do not match numerical simulations. These effects originate from the polarization-sensitive response of the components used to build the setup, especially the beam splitter. Plate beam splitters can have a very different response for each polarization, while cube beam splitters are much better for those measurements; unfortunately, their mounting into a commercial optical microscope requires a custom-made holder.

A simple procedure has been explained to correct for those optical components, such that accurate results are obtained in spite of them. This procedure is based on carefully characterizing each optical component over the entire measurement spectrum. With this procedure, the experimental results match the numerical simulations perfectly. The analysis has been extended to other components in the measurement setup, such as mirrors.

The procedures described here are simple and will enable the accurate spectral measurement of nanostructures, metasurfaces, or any optical component that alters the polarization of the incoming light.

Funding. European Research Council (ERC-2015-AdG-695206); Schweizerischer Nationalfonds zur Förderung der Wissenschaftlichen Forschung (projects 200021_162453).

Disclosures. The authors declare no conflicts of interest.

Data availability. No data were generated or analyzed in the presented research beyond the spectra reported in the figures.

REFERENCES

1. J. Mertz, *Introduction to Optical Microscopy*, 2nd ed. (Cambridge University, 2019).
2. F. Ding, Y. Yang, R. A. Deshpande, and S. I. Bozhevolnyi, "A review of gap-surface plasmon metasurfaces: fundamentals and applications," Nanophotonics **7**, 1129–1156 (2018).
3. J. Scheuer, "Optical metasurfaces are coming of age: short- and long-term opportunities for commercial applications," ACS Photonics **7**, 1323–1354 (2020).
4. M. K. Chen, Y. Wu, L. Feng, Q. Fan, M. Lu, T. Xu, and D. P. Tsai, "Principles, functions, and applications of optical meta-lens," Adv. Opt. Mater. **9**, 2001414 (2021).
5. Y. Deng, Z. Cai, Y. Ding, S. I. Bozhevolnyi, and F. Ding, "Recent progress in metasurface-enabled optical waveplates," Nanophotonics **11**, 2219 (2022).
6. J. Kim, J. Seong, Y. Yang, S.-W. Moon, T. Badloe, and J. Rho, "Tunable metasurfaces towards versatile metalenses and metaholograms: a review," Adv. Photonics **4**, 024001 (2022).

7. H. J. Chen, L. Shao, Q. Li, and J. F. Wang, "Gold nanorods and their plasmonic properties," Chem. Soc. Rev. **42**, 2679–2724 (2013).
8. P. C. Wu, W.-Y. Tsai, W. T. Chen, Y.-W. Huang, T.-Y. Chen, J.-W. Chen, C. Y. Liao, C. H. Chu, G. Sun, and D. P. Tsai, "Versatile polarization generation with an aluminum plasmonic metasurface," Nano Lett. **17**, 445–452 (2017).
9. Y. Cao, L. Tang, J. Li, C. Lee, and Z.-G. Dong, "Four-channel display and encryption by near-field reflection on nanoprinting metasurface," Nanophotonics **11**, 3365–3374 (2022).
10. B. H. Chen, P. C. Wu, V.-C. Su, Y.-C. Lai, C. H. Chu, I. C. Lee, J.-W. Chen, Y. H. Chen, Y.-C. Lan, C.-H. Kuan, and D. P. Tsai, "GaN metalens for pixel-level full-color routing at visible light," Nano Lett. **17**, 6345–6352 (2017).
11. L. Guo, Z. Hu, R. Wan, L. Long, T. Li, J. Yan, Y. Lin, L. Zhang, W. Zhu, and L. Wang, "Design of aluminum nitride metalens for broadband ultraviolet incidence routing," Nanophotonics **8**, 171–180 (2019).
12. A. Leitis, A. Heßler, S. Wahl, M. Wuttig, T. Taubner, A. Tittl, and H. Altug, "All-dielectric programmable Huygens' metasurfaces," Adv. Funct. Mater. **30**, 1910259 (2020).
13. F. Ali and S. Aksu, "A hybrid broadband metalens operating at ultraviolet frequencies," Sci. Rep. **11**, 2303 (2021).
14. P. Zheng, J. Li, Z. Li, M. Ge, S. Zhang, G. Zheng, and H.-C. Liu, "Compressive imaging encryption with secret sharing metasurfaces," Adv. Opt. Mater. **10**, 2200257 (2022).
15. O. Khatib, S. Ren, J. Malof, and W. J. Padilla, "Learning the physics of all-dielectric metamaterials with deep Lorentz neural networks," Adv. Opt. Mater. **10**, 2200097 (2022).
16. Z.-Y. Chiao, Y.-C. Chen, J.-W. Chen, Y.-C. Chu, J.-W. Yang, T.-Y. Peng, W.-R. Syong, H. W. H. Lee, S.-W. Chu, and Y.-J. Lu, "Full-color generation enabled by refractory plasmonic crystals," Nanophotonics **11**, 2891–2899 (2022).
17. H. Liu, H. Peng, K. Li, L. Lu, J. Deng, Y. Liu, C. Qiu, G. Li, and X. Cheng, "Transfer printing of solution-processed 3D ZnO nanostructures with ultra-high yield for flexible metasurface color filter," Adv. Mater. Interfaces **9**, 2101963 (2022).
18. Q. Fan, W. Xu, X. Hu, W. Zhu, T. Yue, C. Zhang, F. Yan, L. Chen, H. J. Lezec, Y. Lu, A. Agrawal, and T. Xu, "Trilobite-inspired neural nanophotonic light-field camera with extreme depth-of-field," Nat. Commun. **13**, 2130 (2022).
19. M. L. Tseng, M. Semmlinger, M. Zhang, C. Arndt, T.-T. Huang, J. Yang, H. Y. Kuo, V.-C. Su, M. K. Chen, C. H. Chu, B. Cerjan, D. P. Tsai, P. Nordlander, and N. J. Halas, "Vacuum ultraviolet nonlinear metalens," Sci. Adv. **8**, eabn5644 (2022).
20. R. Guo, E. Rusak, I. Staude, J. Dominguez, M. Decker, C. Rockstuhl, I. Brener, D. N. Neshev, and Y. S. Kivshar, "Multipolar coupling in hybrid metal–dielectric metasurfaces," ACS Photonics **3**, 349–353 (2016).
21. D. Ray, T. V. Raziman, C. Santschi, D. Etezadi, H. Altug, and O. J. F. Martin, "Hybrid metal-dielectric metasurfaces for refractive index sensing," Nano Lett. **20**, 8752–8759 (2020).
22. J.-H. Yang and K.-P. Chen, "Hybridization of plasmonic and dielectric metasurfaces with asymmetric absorption enhancement," J. Appl. Phys. **128**, 133101 (2020).
23. D. Ray, H.-C. Wang, J. Kim, C. Santschi, and O. J. F. Martin, "A low-temperature annealing method for alloy nanostructures and metasurfaces: unlocking a novel degree of freedom," Adv. Mater. **34**, 2108225 (2022).
24. R. A. Chipman, W. S. T. Lam, and G. Young, *Polarized Light and Optical Systems*, 1st ed. (CRC Press, 2019).
25. S. Sun, K.-Y. Yang, C.-M. Wang, T.-K. Juan, W. T. Chen, C. Y. Liao, Q. He, S. Xiao, W.-T. Kung, G.-Y. Guo, L. Zhou, and D. P. Tsai, "High-efficiency broadband anomalous reflection by gradient meta-surfaces," Nano Lett. **12**, 6223–6229 (2012).
26. C. Yan, K.-Y. Yang, and O. J. F. Martin, "Fano-resonance-assisted metasurface for color routing," Light Sci. Appl. **6**, e17017 (2017).
27. Y. Tan, K. Qu, K. Chen, J. Wu, L. Feng, S. Yang, B. Chen, Y. Wang, C. Zhang, K. Fan, C. Zhang, J. Zhao, T. Jiang, Y. Feng, and B. Jin, "Free-standing single-layer metasurface for efficient and broadband tailoring of terahertz wavefront," Adv. Opt. Mater. **10**, 2200565 (2022).
28. A. Arbabi, Y. Horie, M. Bagheri, and A. Faraon, "Dielectric metasurfaces for complete control of phase and polarization with subwavelength spatial resolution and high transmission," Nat. Nanotechnol. **10**, 937–943 (2015).
29. S. Wang, P. C. Wu, V.-C. Su, Y.-C. Lai, C. Hung Chu, J.-W. Chen, S.-H. Lu, J. Chen, B. Xu, C.-H. Kuan, T. Li, S. Zhu, and D. P. Tsai, "Broadband achromatic optical metasurface devices," Nat. Commun. **8**, 187 (2017).
30. S. Wang, P. C. Wu, V.-C. Su, Y.-C. Lai, M.-K. Chen, H. Y. Kuo, B. H. Chen, Y. H. Chen, T.-T. Huang, J.-H. Wang, R.-M. Lin, C.-H. Kuan, T. Li, Z. Wang, S. Zhu, and D. P. Tsai, "A broadband achromatic metalens in the visible," Nat. Nanotechnol. **13**, 227–232 (2018).
31. P. Chen, B. Fang, J. Li, X. Jing, M. Kong, and Z. Hong, "Enhancement of efficiency on the Pancharatnam–Berry geometric phase metalens in the terahertz region," Appl. Opt. **60**, 7849–7857 (2021).
32. M. Jiang, S. Y. Siew, J. Y. E. Chan, J. Deng, Q. Y. S. Wu, L. Jin, J. K. W. Yang, J. Teng, A. Danner, and C.-W. Qiu, "Patterned resist on flat silver achieving saturated plasmonic colors with sub-20-nm spectral linewidth," Mater. Today **35**, 99–105 (2020).
33. F. Ding, S. Tang, and S. I. Bozhevolnyi, "Recent advances in polarization-encoded optical metasurfaces," Adv. Photonics Res. **2**, 2000173 (2021).
34. Z. Cai, Y. Deng, C. Wu, C. Meng, Y. Ding, S. I. Bozhevolnyi, and F. Ding, "Dual-functional optical waveplates based on gap-surface plasmon metasurfaces," Adv. Opt. Mater. **9**, 2002253 (2021).
35. Z. Yue, J. Li, J. Liu, J. Li, C. Zheng, G. Wang, H. Xu, M. Chen, Y. Zhang, Y. Zhang, and J. Yao, "Versatile polarization conversion and wavefront shaping based on fully phase-modulated metasurface with complex amplitude modulation," Adv. Opt. Mater. **10**, 2200733 (2022).
36. C. Zheng, J. Li, Z. Yue, J. Li, J. Liu, G. Wang, S. Wang, Y. Zhang, Y. Zhang, and J. Yao, "All-dielectric trifunctional metasurface capable of independent amplitude and phase modulation," Laser Photonics Rev. **16**, 2200051 (2022).
37. W. Zhang, B. Gallinet, and O. J. F. Martin, "Symmetry and selection rules for localized surface plasmon resonances in nanostructures," Phys. Rev. B **81**, 233407 (2010).
38. J. Jang, T. Badloe, Y. Yang, T. Lee, J. Mun, and J. Rho, "Spectral modulation through the hybridization of Mie-scatterers and quasi-guided mode resonances: realizing full and gradients of structural color," ACS Nano **14**, 15317–15326 (2020).
39. X. Liu, Z. Huang, and J. Zang, "All-dielectric silicon nanoring metasurface for full-color printing," Nano Lett. **20**, 8739–8744 (2020).
40. W. Yang, S. Xiao, Q. Song, Y. Liu, Y. Wu, S. Wang, J. Yu, J. Han, and D.-P. Tsai, "All-dielectric metasurface for high-performance structural color," Nat. Commun. **11**, 1864 (2020).
41. M. R. Foreman and P. Torok, "Computational methods in vectorial imaging," J. Mod. Opt. **58**, 339–364 (2011).
42. E. Panchenko, L. Wesemann, D. E. Gómez, T. D. James, T. J. Davis, and A. Roberts, "Ultracompact camera pixel with integrated plasmonic color filters," Adv. Opt. Mater. **7**, 1900893 (2019).
43. J. Jang, H. Jeong, G. Hu, C.-W. Qiu, K. T. Nam, and J. Rho, "Kerker-conditioned dynamic cryptographic nanoprints," Adv. Opt. Mater. **7**, 1970016 (2019).
44. C. U. Hail, G. Schnoering, M. Damak, D. Poulikakos, and H. Eghlidi, "A plasmonic painter's method of color mixing for a continuous red–green–blue palette," ACS Nano **14**, 1783–1791 (2020).
45. Q. Dai, N. Zhou, L. Deng, J. Deng, Z. Li, and G. Zheng, "Dual-channel binary gray-image display enabled with Malus-assisted metasurfaces," Phys. Rev. Appl. **14**, 034002 (2020).
46. L. Deng, J. Deng, Z. Guan, J. Tao, Y. Chen, Y. Yang, D. Zhang, J. Tang, Z. Li, Z. Li, S. Yu, G. Zheng, H. Xu, C.-W. Qiu, and S. Zhang, "Malus-metasurface-assisted polarization multiplexing," Light Sci. Appl. **9**, 101 (2020).
47. Y. Zhang, Y. Cheng, M. Chen, R. Xu, and L. Yuan, "Ultracompact metaimage display and encryption with a silver nanopolarizer based metasurface," Appl. Phys. Lett. **117**, 021105 (2020).
48. P. C. Wu, R. Sokhoyan, G. K. Shirmanesh, W.-H. Cheng, and H. A. Atwater, "Near-infrared active metasurface for dynamic polarization conversion," Adv. Opt. Mater. **9**, 2100230 (2021).
49. P. Zheng, Q. Dai, Z. Li, Z. Ye, J. Xiong, H.-C. Liu, G. Zheng, and S. Zhang, "Metasurface-based key for computational imaging encryption," Sci. Adv. **7**, eabg0363 (2021).

50. H. Okamoto, "Local optical activity of nano- to microscale materials and plasmons," J. Mater. Chem. C **7**, 14771–14787 (2019).
51. K. Kumar, H. Duan, R. S. Hegde, S. C. W. Koh, J. N. Wei, and J. K. W. Yang, "Printing colour at the optical diffraction limit," Nat. Nanotechnol. **7**, 557–561 (2012).
52. J. S. Clausen, E. Højlund-Nielsen, A. B. Christiansen, S. Yazdi, M. Grajower, H. Taha, U. Levy, A. Kristensen, and N. A. Mortensen, "Plasmonic metasurfaces for coloration of plastic consumer products," Nano Lett. **14**, 4499–4504 (2014).
53. S. J. Tan, L. Zhang, D. Zhu, X. M. Goh, Y. M. Wang, K. Kumar, C.-W. Qiu, and J. K. W. Yang, "Plasmonic color palettes for photorealistic printing with aluminum nanostructures," Nano Lett. **14**, 4023–4029 (2014).
54. X. Zhu, C. Vannahme, E. Højlund-Nielsen, N. A. Mortensen, and A. Kristensen, "Plasmonic colour laser printing," Nat. Nanotechnol. **11**, 325–329 (2016).
55. T. D. James, P. Mulvaney, and A. Roberts, "The plasmonic pixel: large area, wide gamut color reproduction using aluminum nanostructures," Nano Lett. **16**, 3817–3823 (2016).
56. B.-R. Lu, C. Xu, J. Liao, J. Liu, and Y. Chen, "High-resolution plasmonic structural colors from nanohole arrays with bottom metal disks," Opt. Lett. **41**, 1400–1403 (2016).
57. R. Mudachathi and T. Tanaka, "Up scalable full colour plasmonic pixels with controllable hue, brightness and saturation," Sci. Rep. **7**, 1199 (2017).
58. J. Zhao, X. Yu, K. Zhou, X. Yang, and Y. Yu, "Wide-gamut and polarization-independent structural color at optical sub-diffraction-limit spatial resolution based on uncoupled LSPPs," Nano. Res. Lett. **14**, 214 (2019).
59. J. Zhang, R. Wei, and C. Guo, "Simultaneous implementation of antireflection and antitransmission through multipolar interference in plasmonic metasurfaces and applications in optical absorbers and broadband polarizers," Nanophotonics **9**, 4529–4538 (2020).
60. M. F. Shahin Shahidan, J. Song, T. D. James, and A. Roberts, "Vivid plasmonic color under ambient light," Opt. Express **29**, 40710–40720 (2021).
61. S. L. Lipson and H. Lipson, *Optical Physics*, 4th ed. (Cambridge University, 2010).
62. P. B. Johnson and R. W. Christy, "Optical constants of the noble metals," Phys. Rev. B **6**, 4370–4379 (1972).